Appl. Phys. B 62, 583–599 (1996)

Applied Physics B Lasers and Optics

A detailed rate equation model for the simulation of energy transfer in OH laser-induced fluorescence

R. Kienle, M. P. Lee, K. Kohse-Höinghaus*

Institut für Physikalische Chemie der Verbrennung, Deutsche Forschungsanstalt für Luft- und Raumfahrt e. V., Pfaffenwaldring 38-40, D-70569 Stuttgart, Germany
(Fax: + 49-711/686-2349)

Received: 26 June 1995/Accepted: 17 November 1995

Abstract. A rate equation model (the LASKIN program packet) has been developed for the detailed computation of energy transfer in Laser-Induced Fluorescence (LIF). Calculations of this type are necessary for analysis of the influence of energy transfer processes [e.g., electronic quenching and Rotational Energy Transfer (RET)] on the fluorescence signal. The model has been utilized to examine linear LIF in the OH $A^2\Sigma^+$-$X^2\Pi$ (0, 0) band. Available data on quenching, RET and spontaneous emission rates for the (A, $v' = 0$) state have been reviewed, and models for the state-specific RET and quenching rates have been developed. The accuracy of the calculations has been confirmed by comparison with experimental data, and the LASKIN program has been applied to the analysis of potential error sources in the widely applied two-line LIF temperature-measurement technique. Extensions of the model to the examination of saturated LIF, OH A–X (1, 0) and (3, 0) excitation and LIF of other species (e.g., O_2 and NO) are discussed.

PACS: 34.00

Laser-Induced-Fluorescence (LIF) techniques based upon excitation of the hydroxyl radical (OH) have been widely developed for the study of combustion. The importance of OH as a chemical intermediate, combined with its relatively high concentration in flame zones and its strong radiative transitions in the ultraviolet, makes it one of the leading candidates for quantitative and non-intrusive measurements using laser-based techniques. Single-point and 2-D laser-induced fluorescence of the OH $A^2\Sigma^+$–$X^2\Pi$ band system has been successfully applied to the study of a variety of combustion environments [1, 2].

* To whom all correspondence should be addressed. Fakultät für Chemie, Universität Bielefeld, Universitätsstrasse 25, D-33615 Bielefeld, Germany
(Fax: + 49-521/106-6027)

The measurement of the local OH concentration or rotational temperature with laser-induced fluorescence relies upon a proportionality between the fluorescence intensity and the concentration of the OH radical in the lower laser-coupled energy level. For the case of linear excitation (i.e., no saturation of the excitation transition), the fluorescence is independent of the energy transfer in the ground state, and this proportionality can be expressed in terms of the fluorescence yield in the upper state. This quantity reflects the fraction of molecules promoted to the excited state which undergo radiative decay back to the ground state. It is influenced by a number of factors, including the rates for spontaneous emission (as given by the Einstein A coefficients) and for collisional energy transfer processes such as quenching, Vibrational Energy Transfer (VET) and Rotational Energy Transfer (RET). Thus, the fluorescence yield is in general a complex function of pressure, temperature, chemical composition and the distribution of OH molecules throughout the large manifold of rovibronic energy levels.

One possible method for quantification of fluorescence signals is the experimental determination of the fluorescence yield at every measurement point. Such measurements may be possible for single-point studies, but in general are impractical for multi-point (2-D or 3-D) measurements. In these cases, quantification of OH LIF signals can only be performed under special circumstances. For instance, temperature can be measured using LIF by exciting from two different energy levels in the lower state to the same upper rovibronic state [3], or a combustion environment can be chosen such that the fluorescence yield is approximately constant throughout the measurement area. However, such techniques generally have reduced sensitivity or low signal-to-noise ratio, or they may only be applicable to a limited range of flows.

In general, a detailed computer model is required to examine systematically the influence of the various energy transfer processes on the OH fluorescence yield and signal. In turn, a quantitative analysis is only possible when the rate coefficients for all important energy transfer processes and the chemical composition at the measurement location are known. However, a computer model is very

useful for the examination of sources of measurement error in the application of various LIF techniques. Accurate modelling can also assist in the selection of an experimental approach which is best-suited for a specific combustion environment.

The desire for accurate simulation of the energy transfer dynamics in OH following laser excitation has motivated the development of number of computer models. These models are based upon the description of the time-dependent population in each energy level with an Ordinary Differential Equation (ODE) [4]. Each ODE includes contributions to the energy transfer into or out of the respective level. The dimension of the system of ODEs is thus equal to the number of relevant energy levels. Chan and Daily [5, 6] have utilized a set of 31 differential equations for $N \leq 15$ in OH (A, $v' = 0$) to simulate OH fluorescence spectra. The RET coefficients have been assumed to vary exponentially with transferred energy, and parameters for this exponential dependence have been determined from a fit of the RET data of Lengel and Crosley [7]. Crosley and Smith [8] have used a similar approach to determine temperatures from OH fluorescence spectra; it was noted, however, that their approach is not generally valid. Furuya et al. [9] have also utilized the model of Chan and Daily [5, 6] to measure temperature from LIF spectra. Kotlar et al. [10] have applied a multi-level model to simulate the conditions in the exhaust gas of an atmospheric pressure methane flame. In this model, a bath level consisting of all vibrational levels with $v'' > 0$ has been used. Based upon the magnitude of the collisional energy transfer rates, a fraction of the total population accumulates in this level. This bath-level population can then be ignored in the quantitative analysis of LIF signals. Lucht et al. [11] have simulated fluorescence spectra acquired in a 40 mbar $H_2/O_2/N_2$ flame with the use of a multi-level model. In this study, rates for total RET were measured, and an optimized set of 30 parameters for modelling of the state-to-state RET in OH (A, $v' = 0$) was developed.

To date, the most complete model for energy transfer in OH LIF has been developed by Campbell [12–14]. Two hundred and thirty-two differential equations have been used to simulate the rotational levels in three vibrational states for both the $A^2\Sigma^+$ and $X^2\Pi$ electronic levels. Pressure, temperature, laser intensity and the excited transition [to either the (A, $v' = 0$) or (A, $v' = 1$) levels] can be varied. For the individual collisional processes, different modelling approaches can be used. For instance, for the electronic quenching it can be assumed that a quenching transition is equally probable to all states in the electronic ground state, or selection rules similar to those for radiative transitions can be used. For the description of the RET, the model of Chan and Daily [5, 6] has been applied, and the RET in both electronic levels has been simulated with identical coefficients. Deviation from the results of a two-level model has been used as a criterion for the application of specific measurement techniques, e.g., spectrally narrow or broadband detection of the fluorescence signal.

The acquisition of additional data on energy transfer rates in OH and the improved understanding of the physical mechanisms underlying these processes have necessitated the development of more sophisticated models for simulation of OH LIF. The model which will be discussed here differs from previous models in several aspects. First, the rates for rotational energy transfer (RET) are calculated using the Energy-Correlated-Sudden (ECS-EP) law [15–21]. This scaling law permits computation of the entire matrix of state-to-state RET rates for a given collider and temperature with only four parameters. The results for the ECS-EP model have also been compared with the experimental data on RET for a number of species and temperatures. Second, review of the available data on spontaneous emission and quenching rates has resulted in improved models for the variations of these rates with rotational level and temperature. Third, the sensitivity of the model to variations in the rates for specific energy transfer processes has been analyzed, and the model has also been applied to a systematic study of potential error sources in the widely utilized two-line temperature measurement technique.

The model has been applied to the analysis of linear LIF in the OH A–X (0, 0) band. Linear laser-excitation results in no significant depopulation of the ground state, and thus modelling of energy transfer processes in the X state (e.g., RET and VET) is not necessary. In addition, the large energy spacing between (A, $v' = 0$) and (A, $v' = 1$) results in negligible energy transfer from the lower-lying energy state to the higher-lying state, and therefore VET in the A state can also be neglected.

1 Rate equation modelling

Figure 1 presents a schematic illustration of the relevant energy levels and energy transfer processes in linear OH A–X (0, 0) LIF. Note that the ground-state energy levels have been reduced to a simple two-level system consisting of the laser-coupled level x and an ensemble level X. The ensemble level is populated by molecules which are

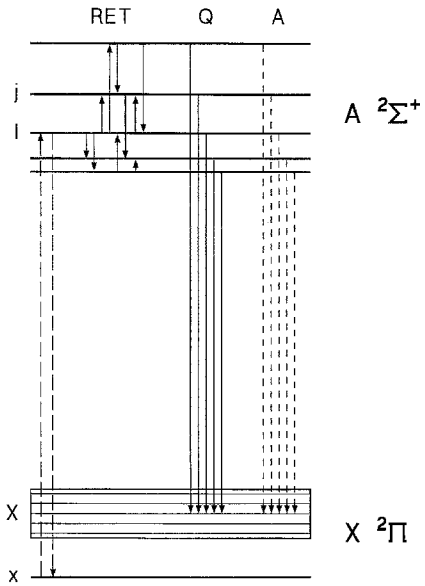

Fig. 1. Schematic diagram of important energy transfer processes in linear OH LIF

electronically quenched from the A state, and there is no transfer out of this state back into the laser-coupled level. The time dependence of the populations in the laser-excited level l, the upper-state levels populated by RET $j \neq l$, and the lower-state levels x and X can be expressed in terms of a system of rate equations:

$$\frac{\mathrm{d}n_l}{\mathrm{d}t} = (B_{xl}n_x - B_{lx}n_l)G_v I_{\mathrm{Las}}(t) + \sum_{j\neq l} R_{jl}n_j - \left(\sum_{j\neq l} R_{lj} + Q_l + A_l\right)n_l, \tag{1}$$

$$\frac{\mathrm{d}n_j}{\mathrm{d}t} = \sum_{i\neq j} R_{ij}n_i - \left(\sum_{i\neq j} R_{ji} + Q_j + A_j\right)n_j \quad (j \neq l), \tag{2}$$

$$\frac{\mathrm{d}n_x}{\mathrm{d}t} = \sum_j (Q_j + A_j)n_j, \tag{3}$$

$$\frac{\mathrm{d}n_x}{\mathrm{d}t} = -(B_{lx}n_x - B_{lx}n_l)G_v I_{\mathrm{Las}}(t), \tag{4}$$

where R_{ij} is the state-to-state rate for RET from level i to level j [s^{-1}], Q_j is the quenching rate [s^{-1}], A_j is the Einstein A coefficient [s^{-1}] and $B_{xl}\ G_v\ I_{\mathrm{Las}}$ and $B_{lx}\ G_v\ I_{\mathrm{Las}}$ are the rates for absorption and stimulated emission, respectively [s^{-1}]. G_v is the spectral overlap integral, representing the overlap between the absorption and laser lineshapes [$1/\mathrm{cm}^{-1}$].

For the purposes of this simulation, the laser pulse shape is assumed to have a temporal dependence of the form

$$I_{\mathrm{Las}}(t) \propto t^a \exp(-bt). \tag{5}$$

Values of $a = 2.5$ and $b = 2\times 10^8\ \mathrm{s}^{-1}$ provide a good approximation of the pulse shape from a typical Nd:YAG laser (pulse duration ~ 10 ns). The rates for quenching (Q_j) and RET (R_{ji}) can be written as a function of n_M [cm^{-3}], the number density of the collision partner M and the collision-partner-specific rate coefficient k[$\mathrm{cm}^3\ \mathrm{s}^{-1}$]:

$$R_{ji} = \sum_M k_{ji}^R(M)n_M, \quad Q_j = \sum_M k_j^Q(M)n_M. \tag{6}$$

n_M can be written as

$$n_M = \chi_M \frac{p}{k_B T}, \tag{7}$$

where χ_M is the mole fraction, p is the pressure, and T is the temperature.

In a typical LIF experiment, the spectrally and temporally integrated fluorescence is often measured. This quantity can be written

$$I_{Fl} = \sum_k A_k \int_0^\infty n_k \mathrm{d}t \tag{8}$$

where the summation extends over all populated rotational levels in the $(A, v' = 0)$ state. Equations (1) and (2) can be integrated to yield

$$n_x B_{xl} G_v \int_0^\infty I_{\mathrm{Las}}\mathrm{d}t - \left(\sum_{j\neq l} R_{lj} + Q_l + A_l\right)\int_0^\infty n_l\,\mathrm{d}t + \sum_{j\neq l} R_{jl}\int_0^\infty n_j\,\mathrm{d}t = 0 \tag{9}$$

$$-\left(\sum_{j\neq l} R_{ji} + Q_j + A_j\right)\int_0^\infty n_j\,\mathrm{d}t + \sum_{i\neq j} R_{ij}\int_0^\infty n_i\,\mathrm{d}t = 0 \quad (j \neq l). \tag{10}$$

Stimulated emission has been neglected under the conditions considered here. Summations of (9) and (10) over all levels j result in the following relation for the time-integrated upper-state population.

$$\sum_k (Q_k + A_k)\int_0^\infty n_k \mathrm{d}t = n_x B_{xl} G_v \int_0^\infty I_{\mathrm{Las}}\mathrm{d}t. \tag{11}$$

The total fluorescence signal I_{Fl} can be written as a function of the fluorescence yield η, which reflects the ratio of the molecules which fluoresce to the total number of excited molecules. The resulting equation is

$$I_{\mathrm{Fl}} = \eta n_x B_{xl} G_v \int_0^\infty I_{\mathrm{Las}}\mathrm{d}t. \tag{12}$$

In general, the fluorescence yield is a complex function of the rates for spontaneous emission and collisional energy transfer. There are a few limits in which the fluorescence yield can be simplified. For instance, when the rates for spontaneous emission and quenching are constant throughout the upper state, the fluorescence yield also reduces to a constant value

$$\eta = \frac{A}{A+Q}. \tag{13}$$

The fluorescence yield can also be simplified in cases where the RET is much slower or much faster than the quenching or spontaneous emission. When the RET is very slow, molecules excited to the upper state remain in the directly excited state until they decay back to the ground state. The fluorescence yield can then be written

$$\eta = \eta_l = \frac{A_l}{A_l + Q_l}. \tag{14}$$

In contrast, when the RET is very fast compared to other energy transfer processes, the population in the upper state will achieve a thermal distribution prior to relaxation back to the ground state. The fluorescence yield is then

$$\eta = \frac{A_{\mathrm{avg}}}{A_{\mathrm{avg}} + Q_{\mathrm{avg}}}, \tag{15}$$

where A_{avg} and Q_{avg} are the thermally averaged rates.

Under typical flame conditions, however, these limits do not apply and a more complex analysis of the fluorescence yield is needed. This analysis requires detailed modelling of the population in each energy level as a function of time. The package of computer programs which has been developed for this purpose takes advantage of the fact that the calculation procedure can be divided into

three separate steps: first, the computation of the energy transfer rates and the construction of the system of ODEs; second, the solution of the ODE system to determine the time-dependent populations in each state; and third, the calculation of the resultant fluorescence signals. Thus, the LASKIN program package consists of three separate program modules. The core of the packet, the ODE solver LASKIN (for LASer KINetics), is a modified version of the LARKIN program, originally developed by Deuflhard et al. [22] for the simulation of large chemical kinetic reaction systems.

2 Inputs to the LASKIN program

A range of spectroscopic data is required to perform calculations of energy transfer in the OH (A, $v' = 0$) state. Term energies and line positions were taken from Coxon [23]. As can be seen in Fig. 2, the values of the Einstein A coefficients in the upper state of OH are somewhat uncertain [24–29]. In particular, variations between experimental studies and theoretical calculations can be observed for low-lying rotational levels. For this study, the Einstein A coefficients were taken from the calculations of Trolier [28], which are in perfect agreement with the results of Luque and Crosley [29].

Accurate computations also require data on state-specific quenching and RET rates. A number of measurements of state-specific and total RET rates have been performed at both low and high temperatures [15–20], and these data have been used to develop the ECS-EP (Energy-Corrected-Sudden) scaling law [21]. With this law, the entire matrix of state-to-state RET coefficients can be specified with just four scaling parameters. However, accurate determination of these parameters requires (at a minimum) state-to-state RET data at low temperatures and total RET data at high temperatures. Such data exist for H_2O, and the ECS-EP law has been shown to model accurately RET of OH in collisions with H_2O across a wide range of physical conditions. To date, the accuracy of the ECS-EP scaling law for other combustion-relevant colliders such as CO_2 and N_2 is unknown, due to the lack of accurate high-temperature RET data for these species. However, as will be discussed below, the combination of low-pressure flame measurements and the application of the LASKIN model has enabled estimation of RET cross sections for these species as well. For helium as collision partner, which may be important as a diluent in some flame studies, the ECS-EP parameters have been determined on the basis of quantum mechanically calculated RET coefficients [17]. For a detailed discussion of the ECS-EP law and the determination of the corresponding parameters, see [21].

A summary of experimental and theoretical data on quenching of OH by H_2O as a function of temperature and rotational level is shown in Fig. 3 [30–39]. For determination of the temperature dependence of the quenching rate, a modified version of the calculations of Garland and Crosley [30] has been used for the LASKIN modelling. As can be seen from Fig. 3a, Garland and Crosley model

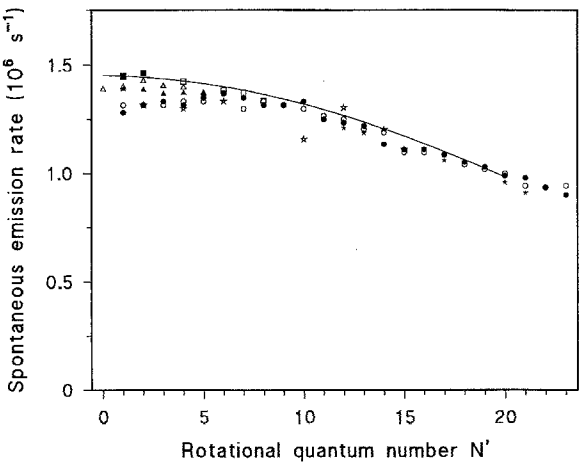

Fig. 2. Spontaneous emission rate from OH(A,$v' = 0$) as a function of rotational level. **Experiment:** *Stars*: [24]; *squares*: [25]; *circles*: [26]; *triangles*: [27]; *open symbols* = $F_1(N')$, filled symbols = $F_2(N')$. **Theory:** *Solid line*: [28] in perfect agreement with [29]

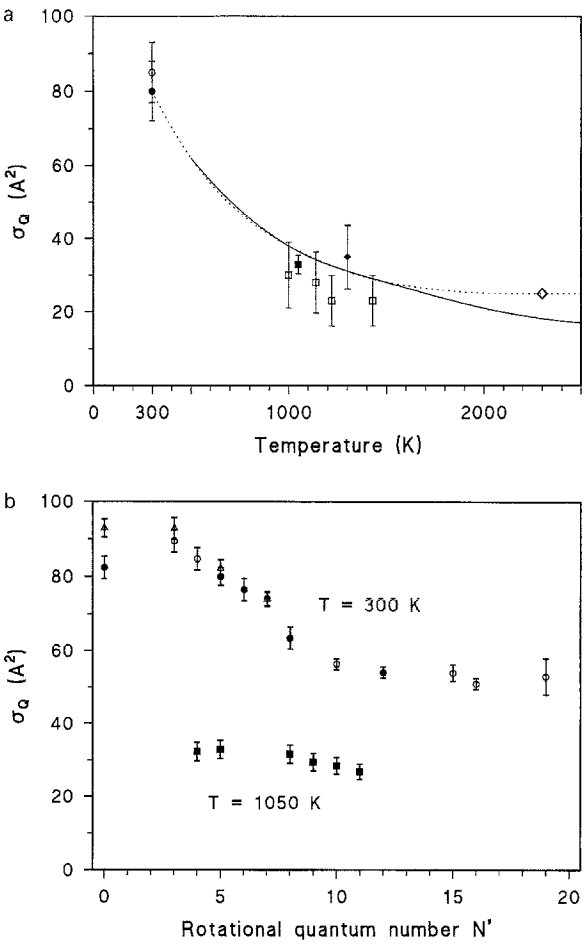

Fig. 3a,b. Cross-section for quenching from OH(A,$v' = 0, 1$) by H_2O. **a** As a function of temperature (for an averaged N'). *Open circle*: $v' = 0$, [36]; *filled circle*: $v' = 1$, [35, 37]; *open squares*: $v' = 0$, [33]; *filled square*: $v' = 1$, [39]; *open diamond*: $v' = 0$, [34]; *filled diamond*: $v' = 0$, [32]; *solid line*: [30]; *dotted line*: value used in this study, in good agreement with *Paul* [31]. **b** As a function of rotational level N'. *Open circles*: $v' = 0$, [37]; *filled circles*: $v' = 1$, [37]; *open triangles*: $v' = 0$, [40]; *filled squares*: $v' = 1$ [39]

accurately the available experimental data on OH quenching by H_2O for temperatures under 1500 K. The discrepancy between the model and the results of Fairchild et al. [33] is consistent with their hypothesis that their measurements represent a lower limit for the quenching cross section. The measurements of Jeffries et al. [34] at 2300 K do appear to show that the Garland and Crosley model underestimates the quenching rate at high temperatures. Thus, for the temperature range above 1500 K, the results of Garland and Crosley have been modified to achieve an agreement between measurement and theory. The recent results of Paul [31] illustrate that this correlation is justified for elevated temperatures. For the collision partner CO_2 and CO, the harpooned model of quenching from Paul [31] has been used, since the results of this model appear to reproduce the available experimental data more accurately than the model of Garland and Crosley. The cross section for N_2 quenching was taken to be negligible, an assumption which is questionable at low temperatures but should be valid at the elevated temperatures typically found in flames (Table 1 in [31]).

Most of the studies of electronic quenching as a function of rotational level have been performed at room temperature. These results (with the exception of Papagiannakopoulos et al. [38]) illustrate that the quenching rate tends to decrease with increasing rotational level. The strength of this decrease is dependent on the collision partner. For very high rotational levels ($N' > 10$), it appears that the quenching rate approaches a constant value, at least for H_2O [37].

There have been fewer studies on the rotational-level dependence of the quenching at higher temperatures [34, 37, 39, 40]. Jeffries et al. [34] have measured quenching rates from the $N' = 3$, 8 and 16 levels of OH in a low-pressure flame with H_2 as the fuel and a varying mixture of O_2 and N_2O as the oxidizer. By altering the oxidizer mix, the temperature in the flame could be varied from 1200 to 2300 K. The results illustrate that the variations in the quenching rate with rotational level are smaller with increasing temperature. It should be noted that due to the varying gas mixture in this flame, it is not possible to relate the measured quenching rate directly to a specific collision partner such as H_2O.

The lifetime measurements of Cattolica and Mataga [39] for the $v' = 1$ state of OH also provide insight into the rotational-level dependence of the quenching rate in the A state of OH. These results illustrate that the quenching cross section for H_2O decreases 17% from $N' = 4$ to $N' = 11$ at 1050 K.

An important problem in the proper interpretation of the measurements of quenching rate with rotational level should not be ignored: quenching rates are typically determined by exciting a specific energy level and then measuring the broadband fluorescence decay time (the decay time from the entire upper state). However, RET in the upper state acts to redistribute the population from the initially excited level to other levels in the upper state. Thus, the quenching rate which is typically measured is not the state-specific rate, but rather the rate following partial thermalization of the population over a wide range of states. The determination of the state-specific rate, which is required by the LASKIN program, requires analysis of the measured quenching rates in combination with the RET rates.

Copeland et al. [40] have proposed the following empirical relation for the room-temperature state-specific H_2O quenching rate $k^Q_{N'}$ from the excited state as a function of the state-specific quenching rate from the lowest-lying rotational state k^Q_0:

$$k^Q_{N'} = k^Q_0 \exp[-aN'(N'+1)]. \tag{16}$$

An alternate form was also examined:

$$k^Q_{N'} = k^Q_0 \exp(-aN'). \tag{17}$$

There is no theoretical basis for either of these functional dependences. The ability of these relations to replicate the variation of the quenching rate with rotational level was examined by combining computed rotationally averaged quenching rates (calculated using the LASKIN program) with lifetime measurements acquired following excitation of several rotational levels in the OH (A, $v' = 0$) state in the exhaust gases of a 25 mbar H_2/O_2/He flame at 1360 K [20]. These model calculations include quenching and RET due to collisions with the major constituents of the exhaust gases. The simulations showed that the functional dependence of the state-specific quenching rate shown in (17) leads to a significantly better representation of the measured fluorescence decay rates compared to the dependence in (16).

The results for the representation in (17) are shown in Fig. 4. Three different decay rates are given in Fig. 4a: the state-specific decay rate $Q_{N'} + A_{N'}$, the decay rate $(C_T)_{ave}$ of the total upper-state population, and the total (broadband) fluorescence decay rate $(C_{Fl})_{ave}$. The first, state-specific rate shows the exponential decrease with increasing rotational level according to the dependence in (17). It cannot be measured, since RET leads to a partial redistribution of the population in the upper-state rotational manifold. The total population in the upper state is given by

$$n_T(t) \equiv \sum_k n_k(t). \tag{18}$$

Its decay rate $(C_T)_{ave}$ can be expressed by

$$n_T(t) \propto \exp[-(C_T)_{ave} t]. \tag{19}$$

As seen in Fig. 4a, the functional dependence of this quantity on rotational level is slightly different. If a level with low rotational quantum number is excited, RET acts to shift population to higher-lying levels and vice versa. Considering the decrease of the state-specific quenching coefficient with rotational level, these tendencies lead to the observed behavior with $((C_T)_{ave} < Q_{N'} + A_{N'}$ for low quantum numbers and the opposite for the higher levels.

However, $(C_T)_{ave}$ is also not accessible in the experiment. Rather, the broadband fluorescence is measured with contributions of individual emissions from the populated rotational levels

$$I_{Fl}(t) \equiv \sum_k A_k n_k(t). \tag{20}$$

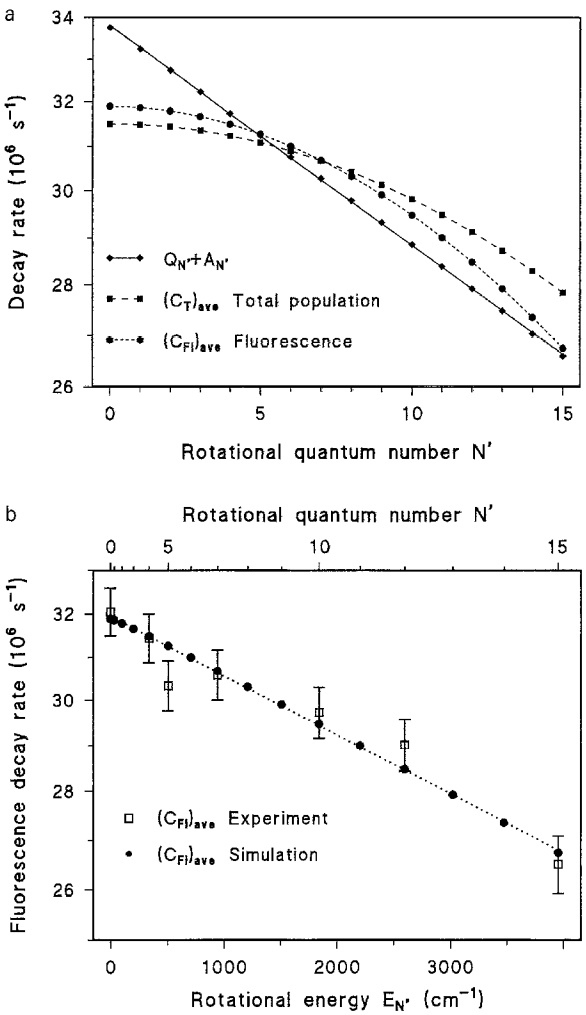

Fig. 4a,b. Quenching from OH (A, $v' = 0$) in the exhaust gases of a H_2/O_2/He flame (25 mbar). Note the logarithmic scale of the y-axis on both plots. **a** Simulation. Decay rate as a function of rotational level. $Q_{N'} + A_{N'}$ state-specific rate for deactivation; $(C_T)_{ave}$: effective decay rate for the total population in $v' = 0$; $(C_{Fl})_{ave}$: effective decay rate for the broadband fluorescence. **b** Comparison with experiment. Fluorescence decay rate $(C_{Fl})_{ave}$ as a function of rotational energy and rotational level; note that the decay rate decreases exponentially with increasing rotational level

Due to the variation in the Einstein A coefficients in the upper level, the total fluorescence decay rate $(C_{Fl})_{ave}$ given by

$$I_{Fl}(t) \propto \exp[-(C_{Fl})_{ave}\, t] \tag{21}$$

is not identical to $(C_T)_{ave}$ (Fig. 4a).

Figure 4b shows the comparison of $(C_T)_{ave}$ from experiment and simulation; here, the dependence on rotational energy is given. The agreement is very good. Note that the measured (i.e., partially thermalized) fluorescence decay rate decreases approximately exponentially with increasing rotational *energy*, in contrast to the assumed exponential decrease in the state-specific rate with rotational *level*. From these results, it can be concluded that (17) properly reproduces the rotational-level dependence of the state-specific quenching rate and that the observed exponential decrease of the measured fluorescence decay

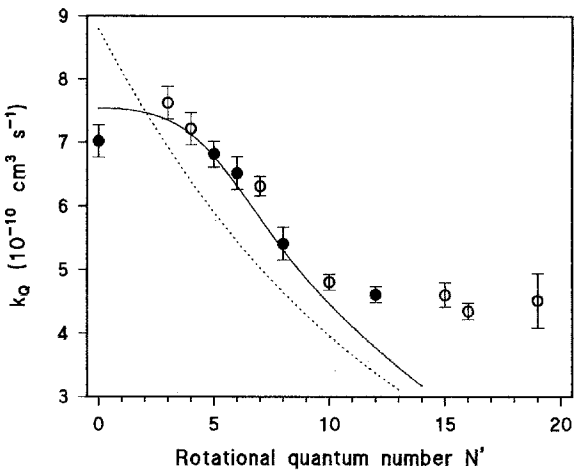

Fig. 5. Quenching from OH(A, $v' = 0, 1$) by H_2O at 300 K ([37]). The discrepancy between the state-specific and effective (i.e., rotationally averaged) quenching rates is due to the thermalizing influence of the RET. **Experiment:** *open circles*: $v' = 0$, *filled circles*: $v' = 1$ **Simulation:** *dotted line*: state-specific quenching rate coefficient; *solid line*: rotationally averaged quenching rate coefficient

rate with rotational *energy* is a result of the rotational redistribution in the excited (A, $v' = 0$) state. The optimal value of the parameter a in (17) is 0.016, corresponding to a decrease in the quenching rate of approximately 1.6% per rotational quantum number. Note that for each collision partner and temperature, a new value for a should be determined.

The variation in quenching rate with rotational level can also be examined by comparison with other measurements. As shown in Fig. 5, comparison of calculations with the detailed quenching measurements of Cleveland and Wiesenfeld [37] for OH (A, $v' = 0$) and (A, $v' = 1$) at 300 K illustrate that an exponential decrease of the state-specific quenching rate with increasing rotational level leads to accurate reproduction of the measured decay rates for $N' \leq 10$. For $N' > 10$, the experimental results show that the dependence of the quenching rate on rotational level disappears. For this temperature, a value for the parameter a of 0.08 for $N' \leq 10$ provides the best agreement between experiment and theory.

The measurements of Jeffries et al. [34] for three rotational levels $N' = 3$, 8 and 16 at temperatures between 1200 and 2300 K were also examined. The results of the LASKIN calculations for this flame are shown in Fig. 6 and can be compared with the data in Fig. 3 of Jeffries et al. [34]. Because only three rotational levels were excited, an exact determination of the a parameter was difficult, but after careful analysis the following values were estimated: $a = 0.02$ (1200 K), $a = 0.012$ (1700 K), $a = 0.007$ (1900 K) and $a = 0$ (for 2300 K). Note that the gas compositions in these flames contain significant concentrations of H atoms and other species, and so the quenching rate (and thus the dependence of this rate on rotational level) cannot be attributed to H_2O alone.

The study discussed here, together with the measurement of Cleveland and Wiesenfeld [37] and Jeffries et al. [34] has examined the rotational-level dependence of the

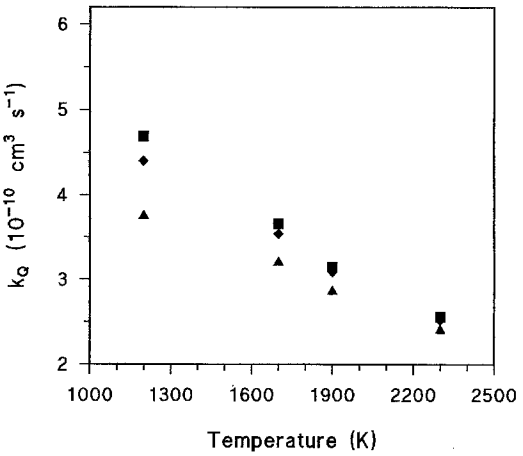

Fig. 6. Quenching from OH(A, $v' = 0$) in the exhaust gases of a H_2 flame with variable temperature. The symbols denote the laser-excited levels (*squares*: $N' = 3$; *diamonds*: $N' = 8$; *triangles*: $N' = 16$). These results can be compared with Fig. 3 in Jeffries et al. [34]

quenching of OH due to collisions with H_2O at temperatures ranging from 300 to 2300 K. In all three studies, a decrease in the quenching rate with increasing rotational level was observed. In addition, the magnitude of this effect decreased with increasing temperature, i.e., the parameter a becomes smaller. Finally, the results presented here illustrate that accurate determination of state-specific quenching coefficients requires the correct simulation of the RET in order to estimate the influence of rotational thermalization on measured quenching rates. Ignoring the influence of this thermalization effect can also lead to an underestimation of the variation of the quenching rate with rotational level.

3 Simulation of H_2 combustion

Temporally integrated fluorescence spectra are particularly useful for a quantitative comparison between experiment and theory. Spectra of this type are relatively sensitive to the relative magnitudes of the energy transfer rates (e.g., to the branching ratio Q_l/R_l) and to RET processes which maintain or change symmetry. In addition, these spectra are not influenced by the details of the laser excitation such as pulse duration and energy. This independence enables comparison of the calculations with spectra which, for practical reasons (e.g., improved S/N ratio), have been measured with high laser intensity. In addition, model results can be compared with experimentally measured spectra from the literature in cases where the details of the laser excitation are not given.

3.1 H_2/O_2/He flames – 25 mbar, 1360 K

As a first application of the LASKIN program, calculations were compared with spectra obtained in a stoichiometric 25 mbar H_2/O_2/He flame (for details on the experimental setup, see [20]). The gas composition in the postflame region was primarily He (54%), H_2O (26%)

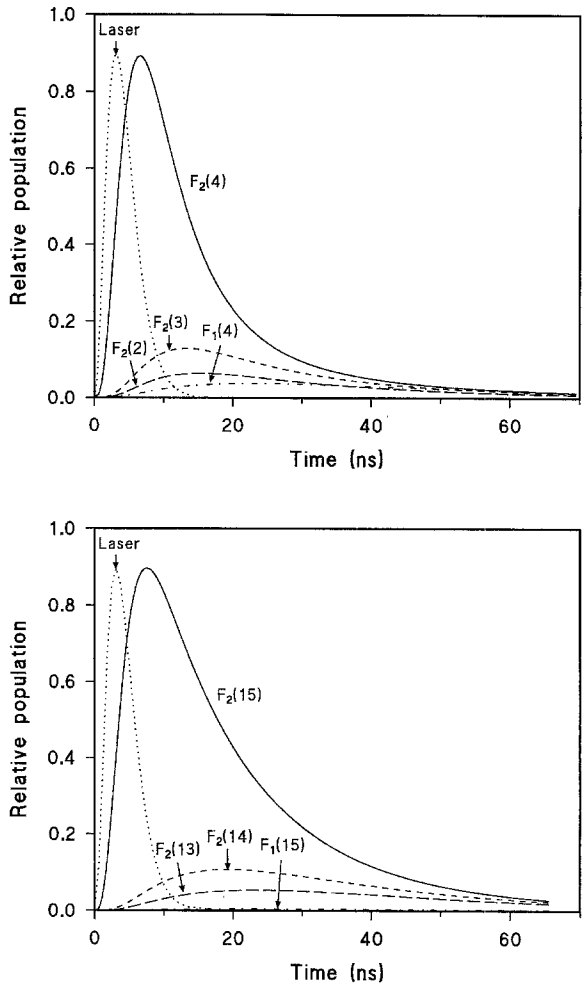

Fig. 7. Simulated population densities for several rotational levels in OH(A, $v' = 0$) in the exhaust gas of a 25 mbar H_2/O_2/He flame. *Upper plot*: Excitation of the $F_2(4)$ level; *lower plot*: Excitation of the $F_2(15)$ level

and H atoms (9%), and the flame temperature at the measurement location in the exhaust gas (48 mm above the burner surface) was 1360 K. The model calculations include the contributions to the RET due to collisions with H_2O and He, and contributions to the quenching due to collisions with H_2O and H atoms. Under these conditions, collisions with H_2O contribute the majority of the quenching and RET. Thus, comparison of experiments and theory provides (to a first order) a test of the accuracy of the modelling of OH–H_2O energy transfer.

For the state-specific quenching rates, an exponential decrease with increasing rotational quantum number [(17), $a = 0.016$] was used. The RET was modelled using the ECS-EP scaling law.

The first step in the simulation was to calculate the time-dependent populations in the upper-state rotational levels following laser excitation. Figure 7 illustrates the populations in several levels following excitation of the $F_2(4)$ and $F_2(15)$ transitions. Temporal integration of these profiles (from $t = 0$ to 70 ns) results in the population distributions shown in Fig. 8. The dominance of the laser-excited level is clear, as is the greater population

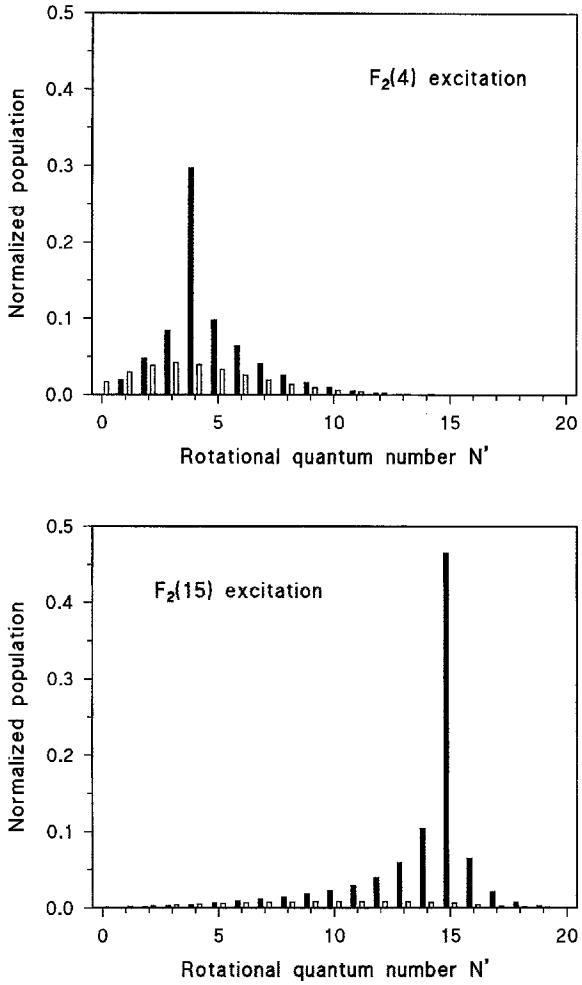

Fig. 8. Simulation of the temporally integrated population densities in OH(A, $v' = 0$) in the exhaust gas of a 25 mbar H_2/O_2/He flame. *Open bars*: F_1 levels; *filled bars*: F_2 levels. *Upper plot*: Excitation of the $F_2(4)$ level; *lower plot*: Excitation of the $F_2(15)$ level

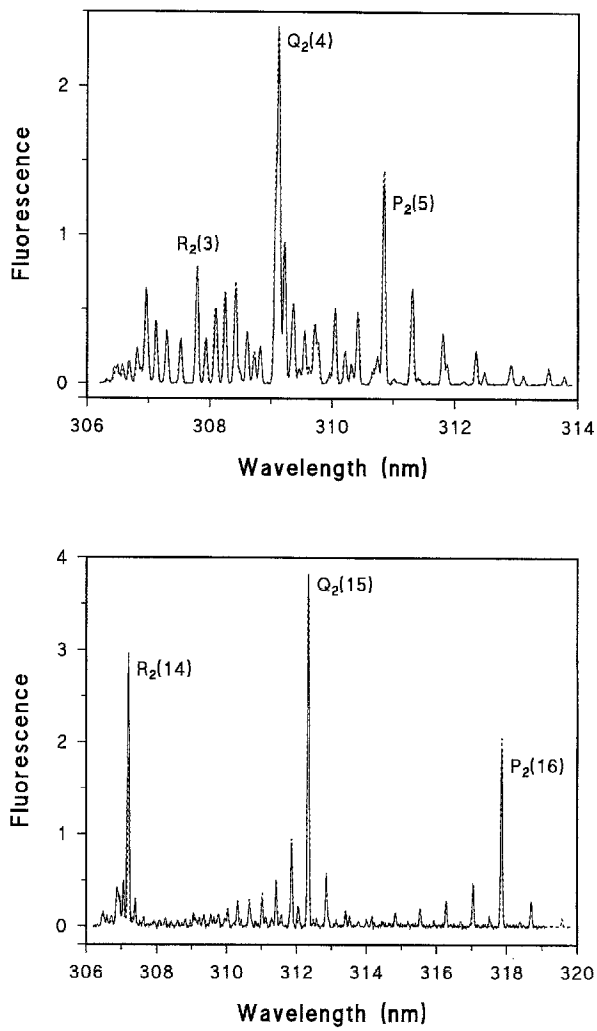

Fig. 9. Comparison of measured and simulated fluorescence spectra from OH($A,v' = 0$) in the exhaust gas of a 25 mbar H_2/O_2/He flame. *Solid line*: experiment; *dashed line*: simulation. *Upper plot*: Excitation of the $F_2(4)$ level; *lower plot*: Excitation of the $F_2(15)$ level

in the F_2 fine-structure components compared to the corresponding F_1 components. This difference is a direct result of the tendency towards conservation of fine-structure component or *e/f* symmetry for RET of OH in collisions with H_2O (i.e., $F_1 \rightarrow F_1$ and $F_2 \rightarrow F_2$ transitions are more likely than $F_1 \rightarrow F_2$ and $F_2 \rightarrow F_1$ transitions) [16,17].

The temporally-integrated population distributions can then be combined with the Einstein A coefficients to calculate fluorescence spectra. The comparison of calculated and measured spectra for the two excitations is shown in Fig. 9. In general, very good agreement between model and theory is observed. Note that the fluorescence spectra are dominated by three strong transitions $R_2(N'-1)$, $Q_2(N')$ and $P_2(N'+1)$ originating from the laser-excited level $F_2(N')$. In the experiment, excitation of the $R_2(14)$ transition was used to populate the $F_2(15)$ level. Scattered laser light at this wavelength results in the anomalously large peak in the measured spectrum.

Fluorescence spectra were also acquired following excitation to the $N' = 0$, 5, 7, 10 and 12 states and compared to LASKIN calculations. A good agreement between experiment and theory was also seen for these transitions. Because of the dominance of H_2O as the primary energy transfer partner for OH in this low pressure flame, these results serve as confirmation of the accuracy of the modelling of energy transfer for OH in collisions with H_2O.

3.2 $H_2/O_2/M$ flames – 50 mbar, 1530 K

The good agreement between the calculations and measurements in the 25 mbar flame verifies the accuracy of both the LASKIN program and the H_2O quenching and RET rates which were utilized as inputs. The LASKIN program can now be combined with additional measurements to examine the RET rates for CO_2 and N_2. This has been performed by examining fluorescence spectra acquired in a stoichiometric 50 mbar $H_2/O_2/M$ flame (M = He, N_2, CO_2). LASKIN was then used to simulate the spectra for a range of N_2 and CO_2 RET rates, in order to determine the rates which gave the best agreement between experimental and theoretical spectra.

The experimental setup was similar to the apparatus described in Lee et al. [20]. The total cold gas flow rate was held constant at 8 slm, and the pressure in the flame was increased to 50 mbar to reduce the mole fraction of H atoms. At the measurement location, the flow composition was 57% diluent, 33% H_2O, 4% H_2, 3% O_2, and 3%H atoms (the increased pressure leads to reduced concentrations of radical species). The temperature for all three flames was $\sim$ 1530 K.

For the simulation, only the collision partners H_2O, H (only for quenching) and the diluent M were considered. As was discussed earlier, the quenching cross sections of H_2O were calculated using a modified version of the model of Garland and Crosley [30]. He and N_2 quenching were assumed to be negligible, and the CO_2 quenching was calculated based upon the model of Paul [31]. The quenching cross sections for collisions with H atoms were taken from Jeffries et al. [34] and were assumed to decrease with increasing rotational level in the same manner as the H_2O cross sections.

The RET due to collisions with H_2O and He was modelled similarly as for the H_2/O_2/He flame in Sect. 3.1. For N_2 and CO_2, representation of the RET was more difficult. The ECS parameters for the collision partner N_2 have been determined based upon room-temperature data [18]. However, at typical flame conditions, the RET rates for N_2 are more uncertain than the rates for H_2O, due to the lack of experimental date on total N_2 cross sections at elevated temperatures. A simulation based upon the high-temperature cross section of Stepowski and Cottereau [41] ($\sigma_R \equiv 80\text{Å}^2$) results in a ratio of the population in the laser-excited state to the population in the entire upper state which is significantly lower than the ratio from the spectra measured in this study. A comparison of calculations and measurements results in an estimate of the total RET cross section for OH(A, $v' = 0$,$N' = 5$) in collisions with N_2 of 40Å^2 at the flame temperature of 1530 K.

For simulation of energy transfer in the $H_2/O_2/CO_2$ flame, the ECS parameters for modelling of the CO_2 RET were assumed to be identical to the parameters for N_2 RET. This assumption was necessitated by the lack of an accurate representation for CO_2 RET at elevated temperatures, and can be justified based upon the similar behavior of the N_2 and CO_2 RET coefficients at room temperature [18].

LIF spectra acquired in the three flames following excitation of the $N' = 5$ level in (A, $v' = 0$) are shown in Fig. 10, together with simulated spectra from LASKIN. Close similarities between the three spectra can be observed. This is primarily due to the continuing importance of H_2O as a colliding species in all three flames despite the high mole fraction of diluent. The spectra were simulated with the LASKIN program, and the resultant total RET rates and quenching rates for OH(A, $v' = 0$, $N' = 5$) for all relevant collision partners are summarized in Table 1.

As can be seen in Table 2, the RET and quenching rates result in varying values for the branching ratio Q_l/R_l in the three flames. The branching ratios lead to good agreement between the measured and calculated ratios of the population in the laser-excited state to the total upper-state population, and this agreement serves as further confirmation of the accuracy of the calculation.

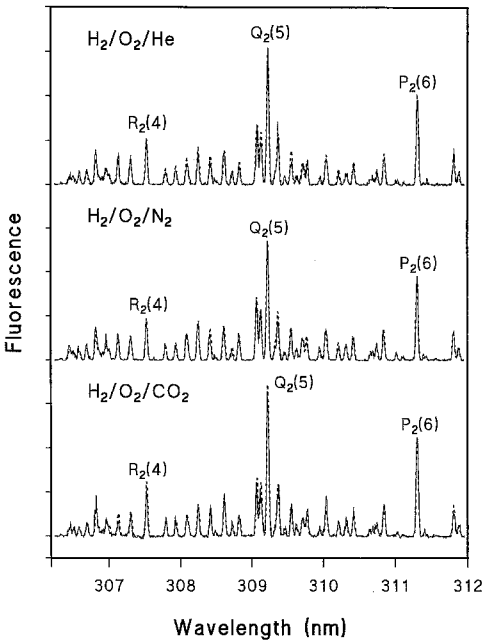

Fig. 10. Comparison of measured and simulated fluorescence spectra from OH(A, $v' = 0$) in the exhaust of a 50 mbar H_2/O_2/M flame (M = He, N_2, CO_2). *Solid line*: experiment, *dashed line*: simulation

Table 1. Estimated energy transfer in OH (A ,$v' = 0$, $N' = 5$) for the simulation of the 50 mbar H_2/O_2/M flame (M = He, N_2, CO_2)

Coll. partner		Total RET		Quenching	
	χ [%]	σ_R [Å^2]	$k_R \chi \cdot n$ [10^6 s^{-1}]	σ_Q [Å^2]	$k_Q \chi \cdot n$ [10^6 s^{-1}]
H_2O	33	150	226	29	44
H	3	—	—	13	5.4
He	57	6.6	29	—	—
N_2	57	40	94	0.6	1.3
CO_2	57	41	92	15	32

Table 2. Branching ratios and temporally integrated population ratios in the 50 mbar H_2/O_2/M flame following excitation of $F_2(5)$

Flame	Simulation		Experiment
	Q_l/R_l	$\int N_l dt / \int N_T dt$	$\int N_l dt / \int N_T dt$
H_2/O_2//He	0.193	0.225	0.227 $\pm$ 0.012
$H_2/O_2/N_2$	0.158	0.198	0.201 $\pm$ 0.016
$H_2/O_2/CO_2$	0.257	0.262	0.225 $\pm$ 0.021

Note that the RET rates for N_2 and CO_2 determined in this study should only be viewed as approximate. More accurate determination requires a measurement environment in which the molecule of interest is the dominant collision partner. Because of the large concentration of H_2O in these H_2 flames, this is not the case. However, these results provide an estimate of the RET rates for N_2 and CO_2 at elevated temperature, and they also

demonstrate the importance of H_2O as a more efficient energy transfer partner for OH than either N_2 or CO_2. Although the H_2O mole fraction is only 33% in the exhaust gases (compared to 57% for N_2 and CO_2), water contributes more than 70% of the total RET.

3.3 H_2/N_2O flames – 9.5 mbar, 2300 K

Computations from the LASKIN program have also been compared with the results of the low-pressure flame study of Jeffries et al. [34]. This analysis permits examination of the LASKIN calculations in a flame with a temperature which is significantly higher than that in the flames previously studied.

The exhaust gas at the measurement location had a temperature of 2300 K and consisted primarily of H_2O (42%) and N_2 (46%). Figure 11 displays the fluorescence spectra which were simulated using the LASKIN program for excitation of the $F_1(3)$, $F_2(8)$ and $F_1(16)$ levels. These spectra can be compared with Fig. 4 in Jeffries et al. [34]. For the computation, the quenching rates were computed from the cross sections of Jeffries et al. and were dominated by collisions with H_2O, due to the low quenching cross section for N_2 [32]. The ECS-EP parameters for H_2O and N_2 determined previously from the lower-temperature studies could be used to model RET at this higher temperature, with the exception that the scaling factor had to be increased in order to maintain a constant cross section for total RET out of the $F_1(0)$ level [$\sigma_R(H_2O) = 180$ Å^2 and $\sigma_R(N_2) = 50$ Å^2] (see [21] for definitions of the ECS parameters and further discussion). The good agreement between the calculated and measured spectra for this high-temperature flame illustrates the ability of the LASKIN program to simulate accurately OH fluorescence signals across a wide range of physical conditions.

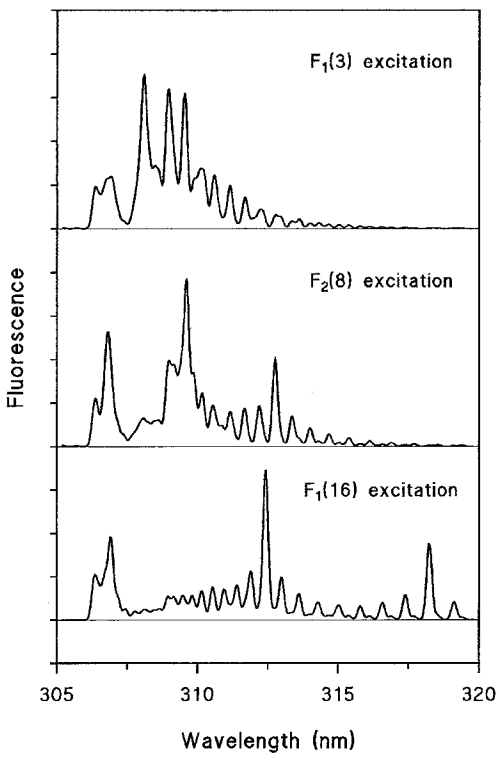

Fig. 11. Simulated fluorescence spectra from OH (A, $v' = 0$) in the exhaust of a 9.5 mbar H_2/N_2O flame. These results can be compared with Fig. 4 in Jeffries et al. [34]

4 Hydrocarbon flames

Following the confirmation of the accuracy of the LASKIN model for predicting energy transfer in hydrogen flames, and the application of the model to the estimation of the N_2 and CO_2 energy transfer rates, LASKIN was utilized for the examination of hydrocarbon flames. Zizak et al. [42] analyzed temporally integrated OH LIF spectra acquired in the exhaust gas of various hydrocarbon flames and determined the population distribution as a function of the laser-excited level. The results from the CH_4/air flame ($\phi = 1.1$, $T = 1950$ K) and the C_2H_2/air flame ($\phi = 1.25$, $T = 2380$ K) are appropriate for comparison with model calculations. A flame modelling program [43] was applied to estimate the species concentrations in the exhaust gases of these flames. For modelling of the energy transfer, the most important species are H_2O, N_2, CO_2 and CO, which constitute 98% of the gas composition. For CO_2, the RET coefficients are uncertain, but are estimated to be similar to the coefficients for N_2; for CO, the RET coefficients are unknown. Because no data on CO is available, the coefficients were assumed to be the same as for N_2. The uncertainty in the RET coefficients for CO and CO_2 has only a small influence on the total RET, because of the dominance of the RET by H_2O and N_2.

In the CH_4/air flame, electronic quenching is dominated by H_2O and CO_2, and in the acetylene flame H_2O, CO_2 and CO are important. The quenching rates for H_2O were chosen based upon the analysis presented previously, the cross sections for CO_2 and CO were taken from the model of Paul [31].

The results of the modelling, together with the data of Zizak et al., are shown in Fig. 12. The time-integrated population distributions illustrate the same characteristics: a marked dominance of the laser-excited rotational level and a tendency for conservation of the fine-structure component. As can be seen by comparison with Fig. 8, these characteristics are not as strong as in the case of the H_2O/He exhaust gas mixture. The good agreement between experiment and calculations for these two flames verifies the validity of both the LASKIN model and the energy transfer rates selected for use in the computations. In particular, the presence of significant quantities of CO_2 and/or CO in these flames (especially the acetylene flame) and the resultant sensitivity of the fluorescence signal to the energy transfer due to these species confirms that the model of Paul [31] simulates accurately the quenching of OH. Application of the model of Garland and Crosley [30] to CO_2 and CO quenching results in much poorer agreement between experiment and theory.

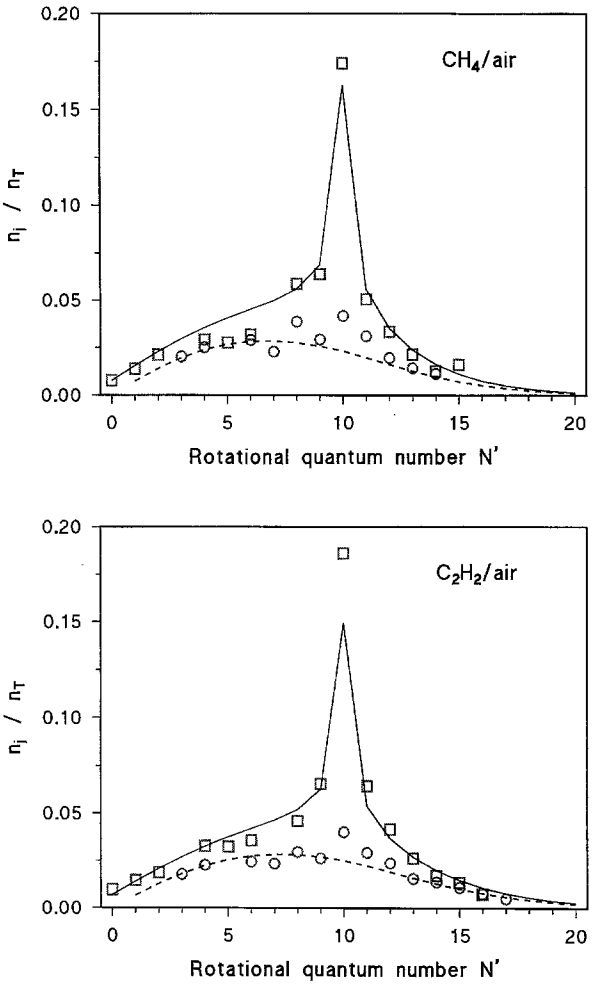

Fig. 12. Comparison of measured and simulated population densities in OH (A, $v' = 0$) following excitation of the $F_1(10)$ level. Experiment (From Zizak et al. [42]): *squares*, F_1 component; *circles*, F_2 component. Simulation: *solid line*, F_1 component; *dashed line*, F_2 component

5 Influence of energy transfer on temperature measurements with linear LIF

Measurement of the rotational distribution of the OH radical with LIF can be used to determine the local temperature in combusting flows. The potential for measurement of 2-D temperature fields with planar LIF is a promising application. However, proper interpretation of the LIF signals relies upon a knowledge of the influence of collisional energy transfer processes upon the fluorescence. The LASKIN program has been used to calculate the potential for these influences to cause errors in temperatures measured using LIF of the OH A–X (0, 0) transition. Note that the calculations have been performed in the limit of linear LIF, and note also that VET between the (A, $v' = 0$) level and other vibrational levels has been neglected. Correct modelling of partially or fully saturated fluorescence will necessitate modelling of RET in the (X, $v'' = 0$) level, and examination of LIF following excitation to higher-lying vibrational states [e.g., (1, 0) or (3, 0)] will require inclusion of the influences of VET in the upper state as well as quenching and RET data for these states.

LIF thermometry relies upon thermal equilibrium in the ground state of the molecule to be probed. In the oft-applied two-line technique, the ratio of fluorescence signals resulting from excitation of two rovibronic transitions is directly related to the populations in the ground states of the transitions through the equation

$$\frac{I_{\mathrm{Fl},1}}{I_{\mathrm{Fl},2}} = \frac{\eta_1 B_1 g_1''}{\eta_2 B_2 g_2''} \exp\left(\frac{E_2'' - E_1''}{k_B T}\right), \tag{22}$$

where η is the fluorescence yield, B is the Einstein coefficient for absorption and g and E are the degeneracy and energy of the lower state. It is assumed that all experimental parameters such as detection efficiency and laser energy are identical for the two measurements.

While the molecular term energies and Einstein coefficients are well-known, the fluorescence yield is a function of the gas composition, pressure and temperature at the measurement location, and, in general, is also a function of the laser-excited state. Because of the difficulty in determining this quantity accurately, variations in the fluorescence yield with rotational level are simply ignored in many applications. In this limit, (21) can be solved to determine the temperature.

$$T_{\mathrm{LIF}} = \frac{E_2'' - E_1''}{k_B} \left(\ln \frac{I_{\mathrm{Fl},1} g_2'' B_2}{I_{\mathrm{Fl},2} g_1'' B_1}\right)^{-1}, \tag{23}$$

This assumption of constant fluorescence yield will generally lead to a systematic error in the measured temperature. The magnitude of this error can be compared using the equation

$$\frac{T_{\mathrm{LIF}} - T}{T} \approx \frac{k_B T}{E_2'' - E_1''} \left(\frac{\eta_2}{\eta_1} - 1\right). \tag{24}$$

Thus, the temperature error depends on the ratio of the fluorescence yields, the choice of excitation lines and the flame conditions.

5.1 Excitation to OH (A, $v' = 0$)

Temperature measurements using LIF of the OH A–X (0, 0) band typically utilize detection of the broadband fluorescence following excitation to the (A, $v' = 0$) level, i.e., the fluorescence is spectrally integrated over the wavelength range encompassing the (0, 0) band. At pressures of 1 atm or higher, the fluorescence decay rate is typically not determined, and the fluorescence signal is then integrated over several fluorescence lifetimes. In contrast, the reduced collision rate in low-pressure flames enables measurement of the fluorescence signal within a time interval which is relatively short compared to the fluorescence lifetime. Thus, depending on the flame environment, OH LIF thermometry can be performed using either temporally resolved or temporally integrated fluorescence detection. Both fluorescence measurement methods will be analyzed in the following sections.

5.1.1 Temporally integrated fluorescence

Model calculations have been performed to determine potential errors in temperature measurements using temporally integrated LIF. As a first step, OH in an environment of pure H_2O at 1 bar was examined. This mixture was chosen for analysis because of the importance of H_2O as a primary energy transfer partner for OH in many flames, and due to the availability of accurate data on H_2O RET and quenching. The ECS-EP parameters for modelling of the RET and the parameter a describing the exponential decrease in the quenching rate with rotational level were taken from the analysis described above.

For determination of the fluorescence yield as a function of rotational level, a laser excitation was simulated for every rotational level from $N' = 0$ to 15. From the state-specific populations, the spectrally and temporally integrated fluorescence was calculated, and these results were used to calculate the fluorescence yield, defined as

$$\eta_l = \frac{I_{\mathrm{FI}}}{n_x B_{xl}}. \tag{25}$$

The fluorescence yield can also be expressed as a function of the rotationally averaged spontaneous emission and quenching rates

$$\eta_l = \frac{\tilde{A}_l}{\tilde{A}_l + \tilde{Q}_l} \approx \frac{\tilde{A}_l}{\tilde{Q}_l}. \tag{26}$$

Figure 13 illustrates a plot of the fluorescence yield [normalized against the fluorescence yield for the $F_1(0)$ state] as a function of rotational level for five different temperatures. The fluorescence yield exhibits a marked dependence on the rotational level at low temperatures, and smaller variations are observed at elevated temperatures. It is also interesting to note that the fluorescence yield decreases with increasing rotational energy for temperatures above $\sim$ 1500 K, and that the opposite behavior is exhibited for lower temperatures.

Variations in the behavior of the fluorescence yield as a function of the temperature and rotational level can be attributed to the influence of these parameters on the rotationally averaged quenching and spontaneous emission rates. At low temperatures, the decrease of the state-specific quenching rate $Q_{N'}$ with rotational level is so pronounced that, despite the decrease in the state-specific radiative decay rate $A_{N'}$ with rotational level and despite the partial thermalization of the population due to RET, the fluorescence yield increases rapidly with rotational level. In contrast, at elevated temperatures the rotational-level dependence of the quenching rate decreases, and the fluorescence yield is then more strongly influenced by the decrease in the Einstein A coefficient. At 1500 K, the variations in $Q_{N'}$ and $A_{N'}$ are roughly equivalent, leading to a nearly constant value for the fluorescence yield. It should be noted that without the redistribution of the rotational population by RET, the rotational-level dependence of the fluorescence yield would be much stronger.

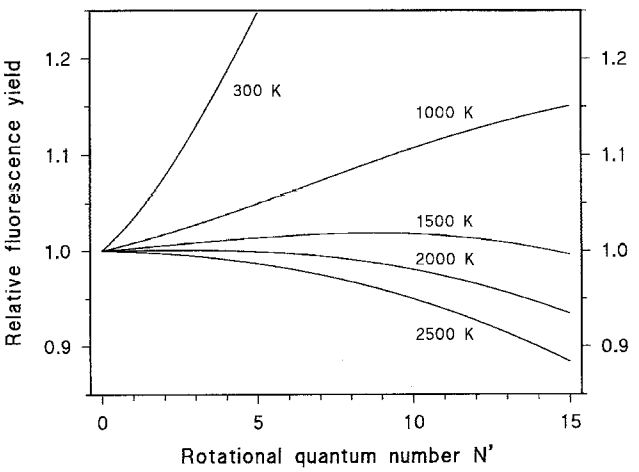

Fig. 13. Relative fluorescence yield as a function of rotational quantum number of the laser-excited state

The accuracy of the two-line technique for temperature measurements was examined by performing calculations of OH LIF signals for five different temperatures ranging from 300 to 2500 K. At each temperature, an appropriate pair of excitation transitions was selected to provide good sensitivity of the signal ratio. For simplicity, all lines were selected from Q_1 branch. The results of the calculations are shown in Table 3.

These "measurement errors" are in agreement with the variations in the fluorescence yield. For low temperatures, the fluorescence yield for the higher-lying level is larger, leading to an overestimation of the temperature, whereas the opposite behavior is observed for elevated temperatures. The percent deviation in temperature is greatest for 300 K ($\sim$ 9%), while for the entire range of flame temperatures the deviation is less than 5%. At 1500 and 2000 K the variation is less than 2%, an unsurprising result in view of the small variations in fluorescence yield at these temperatures (Fig. 13). At 2500 K the largest absolute error is observed, an effect which can be attributed to the variation in the Einstein A coefficient with rotational level.

In the thermometry technique developed by Cattolica [3], the influence of the fluorescence yield on the temperature measurement can be removed by excitation of the transitions $R_1(N-1)$ and $P_1(N+1)$ to the same rotational fine-structure energy level in the $(A, v'=0)$ state. This measurement method will eliminate variations in the fluorescence yield as source of error for OH LIF thermometry. The primary disadvantage of this technique is that the rotational energy spacing of the two ground-state

Table 3. Simulation of temperature measurements for a pure H_2O environment at various temperatures (the parameter a is a measure of the exponential decrease in the quenching rate with rotational level)

T [K]	a	Transitions	T_{LIF} [K]
300	0.08	$Q_1(1)/Q_1(4)$	326
1000	0.03	$Q_1(1)/Q_1(7)$	1045
1500	0.015	$Q_1(1)/Q_1(9)$	1513
2000	0.007	$Q_1(1)/Q_1(11)$	1969
2500	0	$Q_1(1)/Q_1(13)$	2389

energy levels is small, which renders the resulting fluorescence signal ratio relatively insensitive to temperature. This method does, however, demonstrate that the error in the measured temperature will be reduced when the upper-state rotational levels are closely spaced. As an illustration, the LASKIN program has been used to simulate temperature measurements in a pure H_2O environment at 1000 K and 1 bar for excitation of five different line pairs. The ground-state rotational levels in these line pairs are almost identical (variations in fine-structure components only), and the upper-state rotational levels are increasingly separated from each other. The results are shown in Table 4. For excitation to the fine-structure components $F_2(5)$ and $F_1(5)$ via the $S_1(3)$ and $O_2(7)$ lines, the "measured" temperature is in exact agreement with the input temperature, in agreement with the technique proposed by Cattolica [3]. Increasing separation of the upper-state rotational levels leads to increasing errors.

The calculations above have been performed for an atmosphere of 100% H_2O. The simulation can now be extended to an examination of the two-line temperature measurement technique for a gas mixture of 35% H_2O diluted with 65% N_2 or CO_2. Calculations have been performed at 1 bar and temperatures of 1000 and 2500 K, and the results are shown in Table 5.

In the case of the H_2O/N_2 mixture, the rapid RET and low quenching rate for collisions of OH with N_2 leads to a reduction in the branching ratio compared to the pure H_2O environment. This effect leads to more efficient redistribution of the rotational population, and therefore to reduced variations in the fluorescence yield and lower temperature errors.

At room temperature, the quenching rate of OH $(A, v' = 0)$ by CO_2 decreases with increasing rotational level approximately twice as fast as the H_2O quenching rate. A decrease of similar magnitude at 1000 K leads to a temperature error of ~ 80 K, substantially larger than the error for pure H_2O or H_2O/N_2. In contrast, the simulation at 2500 K results in a temperature error which is similar to the error for the other gas mixtures. This effect is due to the reduced variation of the quenching rate with rotational level at elevated temperature, which results in a reduced dependence of the fluorescence signal on collision partner.

These calculations have been performed for a total pressure of 1 bar. In general, the error in OH LIF thermometry due to collisional energy transfer processes is independent of pressure. As long as the energy transfer rates scale linearly with pressure and are large with respect to the spontaneous emission rate, the fluorescence yield will scale linearly with pressure and the ratio η_1/η_2 will be constant. The lower limit of this assumption can be achieved in low-pressure flames, where the quenching is no longer much larger than the radiative decay rate. At elevated pressures, deviations will first be observed when three-body collisions become important. In this regime, the LASKIN model can no longer be applied.

5.1.2 Temporally resolved fluorescence. Rensberger et al. [44] have examined the influence of the temporal detection interval on OH temperature measurements in a 9.5 mbar hydrogen flame. In the exhaust gas of the H_2/N_2O flame, an increased temporal delay of the detection gate (width = 10 ns) with respect to the laser pulse led to a systematic increase in the measured temperature. Temporal gate delays 50 and 250 ns led to variations in the temperature of 80 and 250 K, respectively, in comparison to the temperature measured with a "prompt" gate. In principle, it is not *a priori* possible to say which measurement reflects the true temperature in this flame, although Rensberger et al. [44] have assumed that the temperature measured with the prompt gate (2300 K) is accurate.

The simulation of the energy transfer in this flame has already been discussed in detail (see Sect. 3.3). As Jeffries et al. [34] noted, the variation in the quenching rate with rotational level is negligible in this high-temperature flame. Thus, variations in the detection interval will influence only the RET and spontaneous emission. A simulation of the temperature measurement from Rensberger et al. [44] confirms the dependence of the measured temperature on the delay of the detection gate with respect to the beginning of the laser pulse. For an input temperature of 2300 K, the simulated "measured" temperature varies from 2120 K for 0 ns delay to 2296 K for a 250 ns delay (Fig. 14). The increase in the simulated temperature with increasing delay (Fig. 15a) is in good agreement with the results of Rensberger et al. [44]. The results illustrate, however, that the prompt detection interval – in contrast to the conclusion of Rensberger et al. [44] – provides the poorest reproduction of the input temperature. The largest delay examined here (250 ns) leads to the best agreement between input and output temperatures. When the fluorescence is integrated from 0 to 300 ns (approximately three fluorescence lifetimes), the "measured" temperature is 2203 K, approximately 80 K more than the value measured with prompt detection. This difference is in good

Table 4. Simulation of temperature measurements for a pure H_2O environment at 1000 K

Excitation lines	Transitions	T_{LIF} [K]
$S_1(3)$ $O_2(7)$	$f_1(3)f \rightarrow F_2(5)$ $f_2(7)e \rightarrow F_1(5)$	1000
$R_1(3)$ $P_2(7)$	$f_1(3)e \rightarrow F_1(4)$ $f_2(7)f \rightarrow F_2(6)$	1019
$Q_1(3)$ $Q_2(7)$	$f_1(3)f \rightarrow F_1(3)$ $f_2(7)e \rightarrow F_2(7)$	1035
$P_1(3)$ $R_2(7)$	$f_1(3)e \rightarrow F_1(2)$ $f_2(7)f \rightarrow F_2(8)$	1053

Table 5. Simulation of temperature measurements for various gas mixtures

T [K]	Gas mixture	T_{LIF} [K]
1000	100% H_2O	1045
	35% H_2O, 65% N_2	1034
	35% H_2O, 65% CO_2	1080
2500	100% H_2O	2389
	35% H_2O, 65% N_2	2413
	35% H_2O, 65% CO_2	2395

agreement with the 100 K difference measured by Rensberger et al. [44].

The explanation for this discrepancy is simple. During the first 10 ns following the laser pulse, almost no energy transfer occurs, and thus no redistribution due to RET will be observed. The deviation of approximately 200 K for prompt detection is thus due to the rotational-level dependence of the spontaneous emission. As the delay is increased, the RET leads to a thermalization of the population, and thus this effect is reduced. After ~ 250 ns, the rotational population is nearly equilibrated, and the effective spontaneous emission rate is thus independent of the initially excited rotational level. Thus, the excitation spectrum will accurately reproduce the Boltzmann distribution in the ground state.

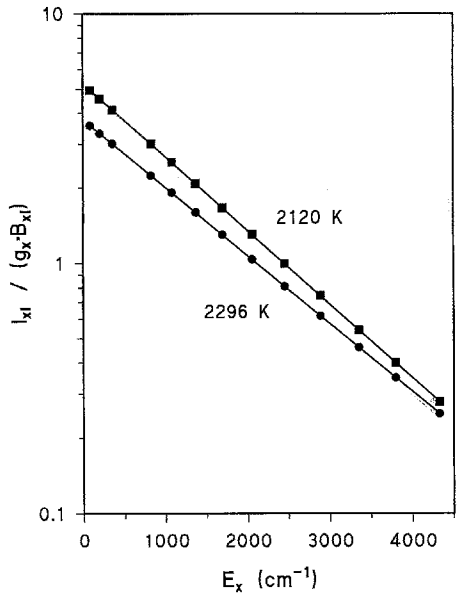

Fig. 14. Simulation of temperature measurements in the exhaust gas of a 9.5 mbar H_2/N_2O flame with variable detection gates. The input temperature is 2300 K. ■, prompt detection interval (0–10 ns); ●, delayed detection interval (250–260 ns)

Jeffries et al. [34] and Rensberger et al. [44] have also examined a H_2/O_2 flame at 9.5 mbar and ~ 1200 K. For this reduced temperature, the variation of the quenching rate with rotational level becomes important. As can be seen from Fig. 15b, variations in the temporal gate delay again lead to variation in the measured temperature. In this case, a prompt detection interval leads to an error of only − 50 K, and a 50 ns delay results in a + 25 K error. Increases in the temporal delay lead to increases in the temperature error. The temporally integrated fluorescence from 0 to 300 ns gives a temperature which is almost exactly correct; in this case, the variations in the quenching and spontaneous emission rates nearly compensate.

These results illustrate that there is no specific temporal detection interval which will always lead to measurement of the correct temperature. When the conditions in the flame to be studied are not well known, a long detection interval is typically the best choice. As the results of this section and the previous section illustrate, temporally integrated LIF measurements typically lead to errors in the measured temperature due to energy transfer processes of less than 100 K throughout the range of typical flame temperatures.

The temporally integrated fluorescence signal can also be corrected for variations in the fluorescence yield. Cattolica and Mataga [39] have measured the fluorescence decay constants in an $H_2/O_2/Ar$ flame and have used these results to correct the measured fluorescence signals. This approach can be utilized to correct for rotational-level-dependent variations in the quenching rates but not the spontaneous emission rates. Thus, this technique is only useful in flames in which the quenching has a greater influence on the fluorescence yield than the spontaneous emission, i.e., only in relatively low-temperature flames. In particular, in moderate-temperature flames, where the variations in the quenching and spontaneous emission tend to cancel, such corrections are not advisable.

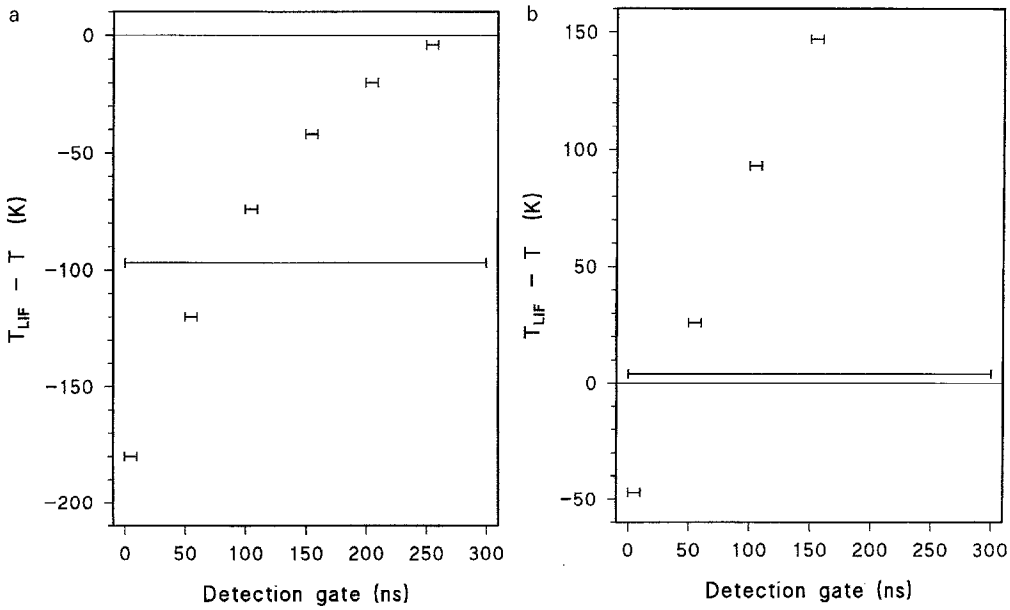

Fig. 15a, b. Influence of the temporal detection gate on the temperature error in an LIF measurement. The *horizontal bars* denote the position and duration of the gate. 0 ns on the horizontal axis corresponds to the beginning of the laser pulse. The temperature error is indicated on the vertical axis. **a** 9.5 mbar H_2/N_2O flame, input temperature = 2300 K. **b** 9.5 mbar H_2/O_2 flame, input temperature = 1200 K

Form the analyses presented above, it can be concluded that errors in temperature measurements using linear LIF of OH are dependent on variations in both the collisional quenching and spontaneous emission rates. In several of the flames analyzed here, it is fortunate that the rotational-level dependences in these quantities partially cancel. In addition, the thermalization due to RET leads to a reduction in the dependence of the fluorescence signal on the initially excited rotational level.

The validity of the results presented here can be summarized. In principle, the model calculations provided accurate information on the general behavior of the temperature error. The exact magnitude of the error is very sensitive to the state-specific quenching and spontaneous emission rates. Although many measurements and calculations of these quantities have been performed, the uncertainties in the dependences on rotational level and temperature remain relatively large, and this limits the absolute accuracy of the calculations. To improve the capability of the calculations, improved data on Einstein A coefficients (in particular for low N') is needed. In addition, quenching rates as a function of N' and temperature for all combustion-relevant temperatures is required. In particular, state-specific quenching rates for CO_2, CO and H_2 at a range of flame temperatures would be helpful. In addition, in many practical flame environments, RET in OH is no longer dominated by collisions with H_2O. In these cases, improved measurements of high-temperature RET rates for collisions with N_2, H_2 and CO_2 are needed. Finally, the accuracy of simulations of OH LIF may decrease in the flame reaction zone, where a large number of atomic and molecular species may contribute to the energy transfer.

6 Extensions of the LASKIN program

To date, the LASKIN program has been applied to analysis of linear laser-induced fluorescence in the OH A–X (0, 0) band. In typical experimental studies, however, other measurement approaches based upon LIF may be applied. Excitation of the (1, 0) transition has often been utilized to reduce the influences of laser absorption and fluorescence trapping. Excitation of the (3, 0) band and the resultant predissociation in the $v' = 3$ level has also been proposed as a technique for reducing or eliminating the influence of collisional energy transfer on the fluorescence signal. In addition, partially or fully saturated fluorescence may be used to maximize the fluorescence signal or to reduce the influence of collisional energy transfer processes. Finally, the development of a computer code which can simulate LIF measurements for other species such as NO and O_2 is also desirable. In principle, the LASKIN program provides the capability to perform simulations for all of these experimental approaches. The program requires, however, accurate data on state-specific rates for all relevant energy transfer processes.

In some flame environments (particularly at pressures of 1 atm or higher), an accurate LIF measurement in the OH A–X (0, 0) band may be problematic due to strong attenuation of the laser energy and trapping of the fluorescence signal. Excitation of the (1, 0) band has been proposed as technique to reduce the influence of these effects. The reduced oscillator strength in the (1, 0) band leads to a reduction in the laser absorption compared to the (0, 0) band, and the capability for detection of the fluorescence in the overlapped (1, 1) and (0, 0) band results in less fluorescence trapping due to the small population in the $v'' = 1$ level in thermal equilibrium. A complete analysis of the energy transfer for this excitation/detection approach requires data on state-specific VET rates from $v' = 1$ to $v' = 0$, RET rates within $v' = 1$ and quenching rates for $(A, v' = 1)$. From previous measurements, it has been observed that the RET [16, 18, 19, 45–47] and quenching [34, 37, 45] rates in $(A, v' = 1)$ are similar to the rates for $(A, v' = 0)$. In contrast, the VET from $v' = 1$ to $v' = 0$ has not been examined in depth. In particular, only one measurement has been performed at elevated temperatures [48], and none of the studies has examined state-to-state VET rates. From the available data, there are indications of large variations in total VET rates with initially excited rotational level [25, 46–48], with species [35] and with temperature [49].

An initial attempt to model the influence of VET on (1, 0) LIF has been performed. The RET and quenching from $v' = 1$ were modelled with the same parameters which were developed for $v' = 0$. In these calculations, the results of Smith and Crosley [48] on high-temperature VET rates have been examined. The data from their study illustrate that, in a lean CH_4/air flame ($\phi = 0.86$) at atmospheric pressure and 1900 K, the VET rate decreases with increasing rotational level (50% decrease from $N' = 1$ to 15). Note that, as in the quenching measurements discussed above, the variations in the VET rate are decreased by the thermalizing effect of RET, and thus the state-specific VET rates must display an even larger variation with rotational level. It was also observed that the population distribution in $(A, v' = 0)$ could be characterized by a thermal distribution (at a different temperature than that found in the flame, however). As input to the LASKIN model, it was assumed that the rotational population in the $(A, v' = 0)$ level following VET is distributed over a wide range of levels and is independent of the initially excited state in $(A, v' = 1)$. Thus, in addition to the 41 rotational fine-structure levels in $v' = 1$, the $v' = 0$ level can be approximated with a single level whose population can be characterized by a thermal Boltzmann distribution. Based upon an examination of the available data on measured VET rates, an exponential fit was performed to estimate the decrease in the state-specific VET rates, similar to that utilized previously for fitting of the quenching rates. This analysis resulted in a relatively large value of $a \sim 0.1$, indicating that the state-specific VET rate decrease approximately 10% per rotational quantum number.

The temporally integrated fluorescence spectra following excitation to OH $(A, v' = 1, N' = 1, 5, 10)$ indicate that the rotational population distribution in $v' = 0$ can be described by a temperature of 2250 K. For excitation of higher-lying rotational levels, this was no longer true. Based upon the assumption of a thermal distribution at 2250 K in $v' = 0$ following $v' = 1$ excitation, temporally integrated fluorescence spectra have been computed for two different excitations and are shown in Fig. 16. These spectra can be compared with Fig. 2 in Smith and Crosley

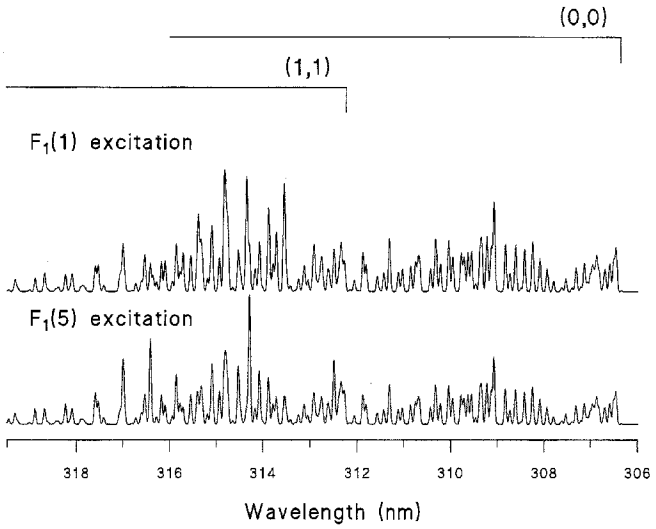

Fig. 16. Simulation of fluorescence spectra following excitation of OH (A, $v' = 1$) in the exhaust gas of a 1 bar CH_4 flame. Note that the wavelength is plotted from right to left. These results can be compared with Fig. 2 in Smith and Crosley [48]

[48]. The good agreement between the spectra can be taken as indication of an accurate simulation. It should be repeated that the RET and quenching were modelled on the basis of the rate coefficients from (A, $v' = 0$) and the estimated concentrations of H_2O, N_2 and CO_2.

The LASKIN program has also been utilized to analyze the accuracy of LIF temperature measurements in this CH_4/air flame. For an input temperature of 1900 K, calculations were performed for excitation of the $Q_1(1)$ and $Q_1(11)$ lines. The spectrally and temporally integrated fluorescence signals were computed and were used to estimate the temperature which would be "measured". For the two transitions, an averaged value of the Einstein coefficient of $1.34 \times 10^6\ s^{-1}$ for the (0, 0) band was used, corresponding to a thermal rotational distribution at 2250 K. The resulting value for the temperature was 1838 K. In contrast, for excitation of the identical lines in the (0, 0) band, the temperature determined using LIF thermometry was 1884 K.

The greater error in the (1, 0) LIF temperature measurement can be largely attributed to the variation in the VET rate with rotational level, coupled with the varying transition probability in the (1, 1) and (0, 0) bands. The averaged Einstein A coefficient is 1.34×10^6 for $v' = 0$, compared to 0.84×10^6 in $v' = 1$ for $Q_1(1)$ excitation and 0.78×10^6 in $v' = 1$ for $Q_1(11)$ excitation. The rapid decrease in the VET rate for the two levels leads to a variation in the effective fluorescence yield. For $Q_1(1)$ excitation, approximately 40% of the fluorescence originates from $v' = 0$ level, while for $Q_1(11)$ excitation this fraction is reduced to 30%.

This analysis provides an indication of the potential of the LASKIN program for modelling LIF in the (1, 0) band of OH. It has been observed that potential errors in LIF temperature measurements with (1, 0) excitation are strongly dependent on the magnitude and behavior of the VET coefficients. Thus, more accurate analysis of LIF in this band requires accurate measurements of state-specific VET rates for a number of combustion-relevant collision partners (e.g., H_2O, N_2 and CO_2) over a wide range of temperature. In addition, the quenching and RET in the (A, $v' = 1$) state should be examined in more detail.

For the analysis of saturated fluorescence, energy transfer in the X state of OH should be examined. Important energy transfer mechanisms may include RET in the (X, $v' = 0$) state, VET between (X, $v' = 0$) and vibrationally excited levels and the distribution of molecules following quenching from the A state back to the X state. These processes may act to replenish the depleted population in the laser-coupled state, and thus may delay the onset of saturation effects. In the current model, which ignores X-state energy transfer, the observation of saturation effects may be taken as a conservative estimate of the saturation limit.

Examination of fluorescence in the (3, 0) band will require modification of the program to include the effects of predissociation. Studies have shown that predissociation acts to minimize the influence of electronic quenching on the OH (3, 0) fluorescence up to pressures of approximately 1 bar [50–52]. It should, however, be noted that RET is often more rapid than quenching, and this influence, combined with the rotational-level dependence in the predissociation rates, may lead to a collision-dependent variation in the LIF signal, 91e-ven at 1 bar. In addition, the increasing number density in high-pressure flames leads to more rapid energy transfer rates, and collisional processes need to be taken into account. In this case, quenching, RET and VET rates from $v' = 3$ and from the cascade of collisionally populated levels below $v' = 3$ (i.e., $v' = 2$, 1 and 0) will be needed [53]. Note that narrowband fluorescence detection techniques (i.e., techniques which utilize spectral filtering to limit the detection bandwidth to a reduced set of rovibronic transitions) may reduce the influence of the energy transfer processes in the collisionally populated energy levels on the fluorescence signal.

For modelling of NO and O_2 LIF [1, 2], conversion of the LASKIN program to computation of these molecules is simple, however, quenching, RET and VET rates in the ground and excited states must be analyzed. For LIF of the O_2 Schumann-Runge band system, this analysis is simplified by the extremely rapid predissociation in the upper state, thus eliminating the need for knowledge of collisional energy transfer rates in this state. Even in this case, however, accurate simulation requires knowledge of the RET and VET rates in the ground state.

7 Conclusions

The LASKIN program packet provides a powerful tool for the modelling of energy transfer in laser-induced fluorescence. The model has been applied to the examination of linear OH A–X (0, 0) fluorescence for a wide variety of flames, collision partners, pressures and temperatures. The good agreement between experimental measurements and theoretical calculations confirms the accuracy of the LASKIN calculations.

LASKIN represents an advance over previous models of this type in several respects. The application of the ECS-EP scaling law enables simple and flexible modelling

of the state-to-state RET coefficients with only four scaling parameters for each collision partner. Available measurements on electronic quenching have been analyzed to estimate state-specific quenching rates from the rotationally averaged data. The influence of collisions with H_2O on the OH fluorescence can be accurately modelled across a wide range of physical conditions. The modelling for N_2 and CO_2 is somewhat less precise due to the lack of sufficient data on energy transfer for these molecules. However, comparison of temporally integrated spectra with measurements permits estimation of RET rates for these species as well.

The LASKIN code has also been utilized to examine error sources in the widely applied two-line thermometry technique. The influence of both electronic quenching and spontaneous emission on LIF temperature measurements has been demonstrated. The rotational-level dependence of these quantities was shown to be particularly important. In measurements of temperature with temporally integrated fluorescence, the variations in the quenching and spontaneous emission rates compensate for each other, thus reducing the temperature error, although only under specific conditions is the temperature error completely eliminated. The RET in the $(A, v' = 0)$ level acts to thermalize partially the rotational population, reducing the magnitude of these effects. An initial study of the LIF thermometry in the A–X (1, 0) band has also been performed, and these results illustrate that, in addition to RET, spontaneous emission and quenching, VET plays an important role in determining the magnitude of the temperature error. More precise analysis of higher-lying transitions such as (1, 0) and (3, 0) will require inclusion of the relevant RET, quenching and predissociation rates, as well as additional data on VET in the OH A state. In addition, modelling of saturated fluorescence will necessitate inclusion of RET and VET rates in the OH X state.

The LASKIN program is available for general distribution from the Deutsche Forschungsanstalt für Luft- und Raumfahrt (DLR). Please contact the author at the Universität Bielefeld for more information.

Acknowledgements. The authors gratefully acknowledge the assistance of Dr. S. Kelm with the flame code calculations. Financial support was provided by the German Ministry of Research and Technology (BMFT) within the research program TECFLAM. Dr. M. Lee would also like to acknowledge financial support from an NSF/NATO Postdoctoral Fellowship and from the DLR.

References

1. A.C. Eckbreth: *Laser Diagnostics for Combustion Temperature and Species* (Abacus, Kent 1988)
2. K. Kohse-Höinghaus: Prog. Energy Combust. Sci **20**, 203 (1994)
3. R.J. Cattolica: Appl. Opt. **20**, 1156 (1981)
4. J. W. Daily: Appl. Opt. **16**, 2322 (1977)
5. C. Chan, J.W. Daily: Appl. Opt. **19**, 1357 (1980)
6. C. Chan, J.W. Daily: Appl. Opt. **19**, 1963 (1980)
7. R.K. Lengel, D.R. Crosley: J. Chem. Phys. **67**, 2085 (1977)
8. D.R. Crosley, G.P. Smith: Combust. Flame **44**, 27 (1982)
9. Y. Furuya, M. Yamamoto, Y. Takubo: Jpn. J. Appl. Phys. **24**, 455 (1985)
10. A.J. Kotlar, A. Gelb and D.R. Crosley: *Laser Probes for Combustion Chemistry*, ACS Symp. Ser. **134**, 137 (American Chemical Society, Washington, DC 1980)
11. R.P. Lucht, D.W. Sweeney, N.M. Laurendeau: Appl. Opt. **25**, 4086 (1986)
12. D.H. Campbell: Appl. Opt. **21**, 2912 (1982)
13. D.H. Campbell: Appl. Opt. **23**, 689 (1984)
14. D.H. Campbell: Appl. Opt. **23**, 1319 (1984)
15. T.A. Griffin, A. Jörg, U. Meier, K. Kohse-Höinghaus: *Proc. 11th Int'l Symp. on Gas Kinetics,* Assisi, Italy (1990)
16. A. Jörg, U. Meier, K. Kohse-Höinghaus: J. Chem. Phys. **93**, 6453 (1990)
17. A. Jörg, A. Degli Esposti, H.-J. Werner: J. Chem. Phys. **93**, 8757 (1990)
18. A. Jörg, U. Meier, R. Kienle, K. Kohse-Höinghaus: Appl. Phys. B **55**, 305 (1992)
19. R. Kienle, A. Jörg, K. Kohse-Höinghaus: Appl. Phys. B **56**, 249 (1993)
20. M.P. Lee, R. Kienle, K. Kohse-Höinghaus: Appl. Phys. B **58**, 447 (1994)
21. R. Kienle, M.P. Lee, K. Kohse-Höinghaus: Appl. Phys. B (submitted)
22. P. Deuflhard, G. Bader, U. Nowak: In *Modelling of Chemical Reaction Systems*, ed. by K.H. Ebert, P. Deuflhard, W. Jäger, Springer Ser. Chem. Phys., Vol. **18**, (Springer, Berlin, Heidelberg 1981)
23. J.A. Coxon: Can. J. Phys. **58**, 933 (1980)
24. R.A. Sutherland, R.A. Anderson: J. Chem. Phys. **58**, 1226 (1973)
25. K.R. German: J. Chem. Phys. **64**, 4065 (1976)
26. J. Brzozowski, P. Erman, M. Lyyra: Phys. Scr. **17**, 507 (1978)
27. I.S. McDermid, J.B. Laudenslager: J. Chem. Phys. **76**, 1824 (1982)
28. M.R. Trolier: Kinetic and spectroscopic studies of ozone photochemistry. Ph.D. Thesis, Cornell University, Ithaca, NY (1988)
29. J. Luque, D.R. Crosley: Private communication (1994)
30. N.L. Garland, D.R. Crosley: *21st Symposium (Int'l) on Combustion* (The Combustion Institute, Pittsburgh, PA 1986) p. 1693
31. P.H. Paul: J. Quant. Spectrosc. Radiat. Transfer **51**, 511 (1994)
32. T. Carrington: J. Chem. Phys. **30**, 1087 (1959)
33. P.W. Fairchild, G.P. Smith, D.R. Crosley: J. Chem. Phys. **79**, 1795 (1983)
34. J.B. Jeffries, K. Kohse-Höinghaus, G.P. Smith, R.A. Copeland, D.R. Crosley: Chem. Phys. Lett. **152**, 160 (1988)
35. R.A. Copeland, M.L. Wise, D.R. Crosley: J. Phys. Chem. **92**, 5710 (1988)
36. I.J. Wysong, J.B. Jeffries, D.R. Crosley: J. Chem. Phys **92**, 5218 (1990)
37. C.B. Cleveland, J.R. Wiesenfeld: Chem. Phys. Lett. **144**, 479 (1988)
38. P. Papagiannakopoulos, C. Fotakis: J. Phys. Chem. **89**, 3439 (1985)
39. R.J. Cattolica, T.G. Mataga: Chem. Phys. Lett. **182**, 623 (1991)
40. R.A. Copeland, M.J. Dyer, D.R. Crosley: J. Chem. Phys. **82**, 4022 (1985)
41. D. Stepowski, M.J. Cottereau: J. Chem. Phys. **74**, 6674 (1981)
42. G. Zizak, J.A. Lanauze, J.D. Winefordner: Combust. Flame **65**, 203 (1986)
43. J. Warnatz: One-dimensional flame code, 1991 version (Institut für Technische Verbrennung, Universität Stuttgart 1991)
44. K.J. Rensberger, J.B. Jeffries, R.A. Copeland, K. Kohse-Höinghaus, M.L. Wise, D.R. Crosley: Appl. Opt. **28**, 3556 (1989)
45. J. Burris, J.J. Butler, T.J. McGee, W.S. Heaps: Chem. Phys. **124**, 251 (1988)
46. R.K. Lengel, D.R. Crosley: Chem. Phys. Lett. **32**, 261 (1975)
47. R.K. Lengel, D.R. Crosley: J. Chem. Phys. **68**, 5309 (1978)
48. G.P. Smith, D.R.Crosley: Appl. Opt. **22**, 1428 (1983)
49. D.R. Crosley: J. Phys. Chem. **93**, 6273 (1989)
50. P. Andresen, A. Bath, W. Gröger, H.W. Lülf, G. Meijer, J.J. ter Meulen: Appl. Opt. **27**, 365 (1988)
51. J.A. Gray, R.A. Farrow: J. Chem. Phys. **95**, 7054 (1991)
52. A. Arnold. B. Lange, T. Bouché, T. Heitzmann, G. Schiff, W. Ketterle, P. Monkhouse, J. Wolfrum: Ber. Bunsenges. Phys. Chem. **96**, 1388 (1992)
53. K.L. Steffens, J.B. Jeffries, D.R. Crosley: Opt. Lett. **18**, 1355 (1993)